

8

Earthquake Source Properties From Instrumented Laboratory Stick-Slip

Brian D. Kilgore¹, Art McGarr¹, Nicholas M. Beeler^{1,2}, and David A. Lockner¹

ABSTRACT

Stick-slip experiments were performed to determine the influence of the testing apparatus on source properties, develop methods to relate stick-slip to natural earthquakes and examine the hypothesis of McGarr [2012] that the product of stiffness, k , and slip duration, Δt , is scale-independent and the same order as for earthquakes. The experiments use the double-direct shear geometry, Sierra White granite at 2 MPa normal stress and a remote slip rate of 0.2 $\mu\text{m/sec}$. To determine apparatus effects, disc springs were added to the loading column to vary k . Duration, slip, slip rate, and stress drop decrease with increasing k , consistent with a spring-block slider model. However, neither for the data nor model is $k\Delta t$ constant; this results from varying stiffness at fixed scale.

In contrast, additional analysis of laboratory stick-slip studies from a range of standard testing apparatuses is consistent with McGarr's hypothesis. $k\Delta t$ is scale-independent, similar to that of earthquakes, equivalent to the ratio of static stress drop to average slip velocity, and similar to the ratio of shear modulus to wavespeed of rock. These properties result from conducting experiments over a range of sample sizes, using rock samples with the same elastic properties as the Earth, and scale-independent design practices.

8.1. INTRODUCTION

In this chapter we determine how and under what circumstances laboratory stick-slip source properties can be compared to those of natural earthquakes. To make such a comparison requires (1) a mechanical understanding of laboratory scale earthquakes (2) an accounting for any contributions to source properties that are unique to the laboratory test, and (3) if source properties are scale dependent, a procedure to extrapolate laboratory source parameters to the Earth. To accomplish the first two goals we designed an experimental program of well-instrumented stick-slip. The experiments access a wider range of fault slip, slip rate, and duration than in prior studies by systematically varying the combined elastic properties

of the fault and testing machine. The approach provides a more detailed view of the mechanics of stick-slip, the nature of the contributions to source properties from the testing apparatus, and allows us the necessary physical understanding to accomplish the third goal of properly relating stick-slip source properties to earthquakes.

The control variable that affects slip, slip rate, and duration in the experiments is the elastic shear stiffness [Walsh, 1971], most often referred to simply as "stiffness" throughout this report. Stiffness is the amount that on-fault shear stress in the direction of slip changes per increment of slip, i.e., the slip derivative of the shear stress on the fault, $k = d\tau/d\delta$, where τ is shear stress and δ is the fault slip. The particular value of stiffness provides fundamental control on the properties of the slip portion of a stick-slip cycle, as we explain here with a simple example in which the fault follows a static-kinetic fault strength relation. In a stick-slip test [Brace and Byerlee, 1966], the fault is loaded at a constant velocity. The fault

¹U.S. Geological Survey, Menlo Park, California, USA

²USGS Cascades Volcano Observatory, Vancouver, Washington, USA

remains stuck for some period of time during which the shear stress increases linearly with time, analogous to a natural earthquake recurrence interval. The rate of shear stress increase during this “stick” phase is the product of the loading velocity and the stiffness. Thus, the stiffness influences the length of the interseismic period, the recurrence time of stick-slip. When the shear stress eventually reaches the static strength, the fault fails, dropping strength to the kinetic level, allowing accelerating slip rate as the elastic strain stored in the rock and testing machine is released. During this “slip” phase, the stress drop is the product of the total slip and the stiffness. Equivalently, the unloading stiffness during the slip phase is the ratio of the static stress drop to total slip, $\Delta\tau/\Delta\delta$, and the stiffness influences the earthquake source properties of stick-slip.

In detail and depending on the particular design and dimensions of the testing machine and the rock samples, the stiffness can predominately reflect the elastic properties and dimensions of the rock samples, those of components of the testing machine, or some combination of both [Shimamoto *et al.*, 1980]. For example, for tests employing bare fault surfaces, loading is often provided by a servo-control system that is configured to load the fault at a constant slip rate, using a moving reference location on the loading column as the position feedback point for control. The position of the servo feedback point relative to the fault surface impacts the stiffness and therefore the stability of the control system. If a fault slip measurement is made directly across the fault, with the sensor mounts very near the fault, and if that measurement is used as the control measurement point, since the rock samples are relatively small and the elastic modulus of the rock sample is high, the loading stiffness is very high, directly reflecting the modulus of the sample material. If instead the fault slip control reference point is elsewhere on the loading column, then the resulting loading stiffness is lower and can reflect a combination of the properties of the machine and the sample material.

In the present study, as in most studies of stick-slip, the rock samples around the fault have high elastic modulus and small dimension, and are too stiff to allow the fault to slide unstably [Johnson and Scholz, 1976]. That is, stick-slip often is difficult to access in laboratory geometries (e.g., “triaxial” and “double direct shear”; see subsequent descriptions) unless the loading system adds compliance in addition to that of the rock samples, resulting in a stiffness that includes compliance from the machine. In particular, while our experiments are conducted under servo-control loading, they are designed to reliably produce stick-slip, in part by using highly polished surfaces with a short slip weakening distance [Dieterich, 1978], and also so that the loading and unloading stiffnesses are approximately identical. These desired

properties are achieved by selecting the value of stiffness that is determined, essentially entirely, by a compliant element placed in the loading column between the control point and the fault, and by placing the control point for loading far from the fault.

A few prior studies have explored the influence of stiffness on laboratory stick-slip and the implications for natural earthquakes. Notably, *Byerlee and Brace* [1968] investigated how rock type, confining pressure, strain rate, and stiffness affect stick-slip behavior in triaxial experiments. In these experiments the loading stiffness was varied between the design stiffness of the apparatus and a value an order of magnitude lower, by adding a compliant fluid column in-line with the hydraulic axial loading. Their experiments showed that the stress drop depends on rock type and confining pressure, but not on stiffness. They concluded that the amplitude of motion from natural earthquakes would increase with depth, vary as a function of rock type, but, consistent with natural scale-independent stress drop, would not vary with stiffness. In contrast, by considering possible scaling between the stick-slip and earthquakes, *Walsh* [1971] noted that the shear stiffness of large earthquakes, the ratio of shear modulus μ to the fault dimension L is 4 to 5 orders of magnitude less than the laboratory stiffness, as measured by stress drop and total slip, $\Delta\tau/\Delta\delta$. As a consequence, *Walsh* [1971] cautioned that experiments at reduced stiffness are needed to determine how and whether stick-slip results can be scaled to natural earthquakes. Though no comprehensive experimental studies have been conducted to date, Walsh’s recommendation that differences in stiffness and in fault dimension must be taken into account in scaling laboratory slip to natural settings has been implemented in a number of applications of stick-slip to earthquakes [McGarr, 1994, 1999].

Similarly, fundamental differences between stick-slip and earthquakes may affect the scaling of laboratory measured event durations to that of an earthquake. Since natural rupture propagation speeds are fixed by the elastic properties of rock, earthquake duration is proportional to fault dimension. For example, assuming a crack-like rupture expanding at 85% of the shear wave speed β , and then arrest proceeding as back propagating shear waves, the rupture duration would be $\Delta t \approx 1.1L/\beta$. There is not always such a straightforward expectation for the duration of laboratory stick-slip. For example, in rupture propagation experiments, slip duration can be much longer than the fault length divided by the wavespeed [e.g., Beeler *et al.*, 2012]. This is because the ends of the fault are not confined; instead of the slip beginning to slow down when the rupture front reaches the unconfined end of the fault, the slip continues. And in this case, stick-slip duration is relatable to the resonance period of the testing machine [Johnson and Scholz, 1976],

which may not be controlled directly by the dimensions of the fault itself. Therefore, as with stiffness, there is an expected difference in duration between the lab and field because laboratory fault dimensions are not always explicitly tied to the elastic properties of the mechanical system. Since other earthquake source properties such as slip velocity and acceleration depend on the event duration, more generally, scaling of laboratory stick-slip to natural events requires an understanding of interactions between the on-fault source and the testing machine. Experimentally determining those interactions is a primary part of first of the three goals of this study, as described at the outset of this introduction.

Recent progress by *McGarr* [2012] relating stick-slip to earthquakes provides the most immediate motivation for the experiments and analysis of our study. *McGarr* [2012] uses data from rupture propagation experiments of *Lockner and Okubo* [1983] and *Johnson and Scholz* [1976] to advance two hypotheses: (1) while stick-slip stiffness and event duration might be individually expected to differ substantially from those of natural earthquakes of the same fault dimension, the products $k\Delta t$ for earthquakes and for stick-slip are scale independent, and (2) the products $k\Delta t$ for stick-slip and earthquakes are the same

order of magnitude. That the product is scale independent for earthquakes is expected from simple models of rupture propagation and arrest and is consistent with observed earthquake source properties, as follows. Combining the expected duration of the crack propagation and arrest model described above with *Walsh's* [1971] dimensional relation for stiffness leads to the product being approximately the ratio of elastic material properties, the shear modulus to the shear wave speed,

$$k\Delta t \approx 1.1 \frac{\mu}{\beta}. \quad (8.1a)$$

For shorthand, throughout the remainder of this chapter, we refer to this ratio of the modulus and wave speed as the impedance. Here taking the ratio to be on the order of 10 MPa s/m (e.g., $\mu = 30$ GPa, $\beta = 3$ km/s), the product (8.1a) is around 11 MPa s/m, consistent with seismological data (Figure 8.1a). Stick-slip values of the product are similar (Table 8.1). *Johnson and Scholz* [1976] measured duration and stiffness directly in rupture propagation experiments on a 20 cm long fault and found $k = 12$ GPa/m, $\Delta t = 1$ ms, and the product to be approximately 12 MPa s/m. In experiments on a 2 meter fault,

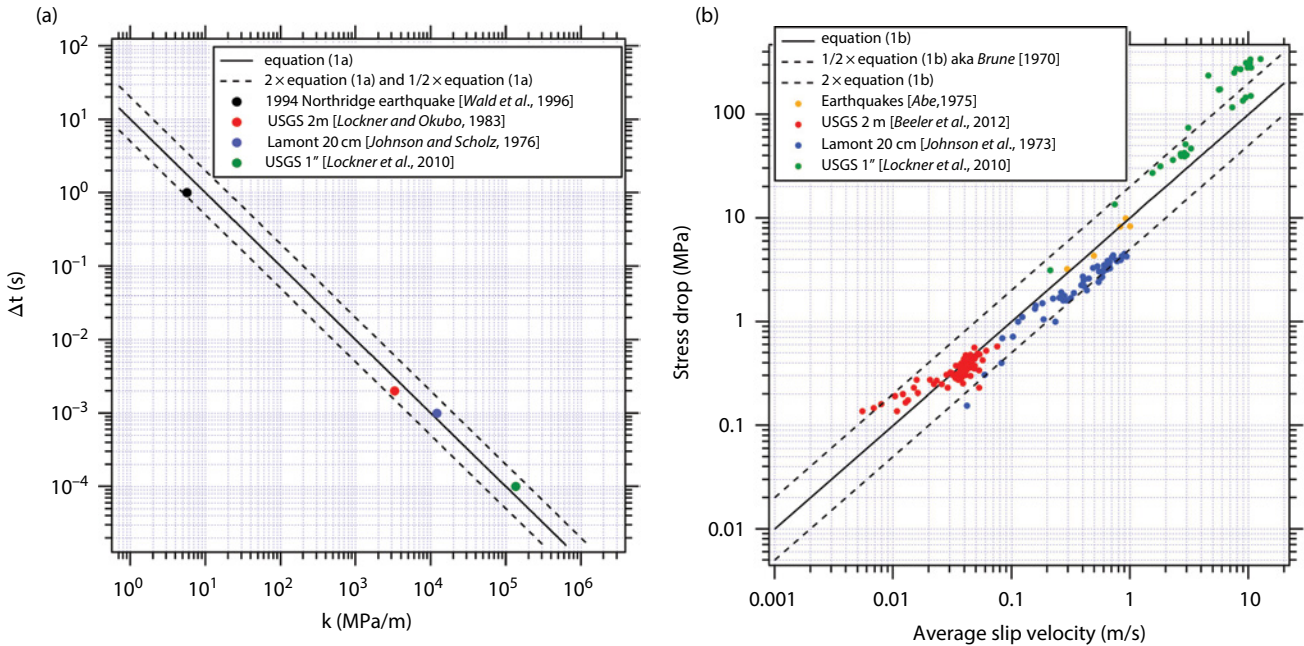


Figure 8.1 Scale-independent laboratory and earthquake source properties. (a) Duration versus stiffness for stick-slip in three testing machines [*Johnson and Scholz*, 1976; *Lockner and Okubo*, 1983; *Lockner et al.*, 2017] and for a typical earthquake [*Wald et al.*, 1996]. The solid line is the scale-independent prediction, equation (8.1a) with the impedance $\mu/\beta=10$ MPa s/m, and the two dashed lines are one half and two times equation (8.1a). (b) Static stress drop versus average slip velocity. Data for individual stick-slip events are shown for the three testing machines in part (a) [*Johnson et al.*, 1973; *Beeler et al.*, 2012; *Lockner et al.*, 2017] and from five Japanese earthquakes [*Abe*, 1975]. The solid and dashed lines are as in part (a). The lower dashed line is equivalently the prediction of the Brune model [*Brune*, 1970].

Table 8.1 Testing machine properties.

Apparatus	Δt (ms)	Stiffness (GPa/m)	$k\Delta t$ (MPa s/m)	Sample Mass (kg)	Fault Area (m^2)	Sample Dimension (m)	Estimated Sample $k\Delta t$ (MPa s/m)
Lamont 20 cm biaxial	1.2	10	12	1.46	0.006	0.18	30.5
USGS 2 m biaxial	2	3.3	6.6	2430	0.8	1.5	37.4
USGS 1 inch triaxial	0.1	135	13.5	0.087	0.001013	0.064	30.5
USGS DDS (this study)	0.5	27	13.5	0.432	0.005	0.08	27.3

Note: DDS=double direct shear configuration.

Lockner and Okubo [1983] found $k = 3.3 \text{ GPa/m}$, $\Delta t = 2 \text{ ms}$, and the product is 6.6 MPa s/m (Figure 8.1a). More recently, *Lockner et al.* [2010, 2017 (this volume)] conducted room temperature stick-slip experiments on a 5 cm long granite fault at elevated confining pressure in a triaxial geometry and found $k = 135 \text{ GPa/m}$, $\Delta t = 0.1 \text{ ms}$, and the product is 13.5 MPa s/m .

Furthermore, *Johnson and Scholz* [1976] note that the product can also be expressed using more standard earthquake source properties as

$$k\Delta t \approx \frac{\Delta\tau_s}{\hat{V}}, \quad (8.1b)$$

where $\hat{V} (= \Delta\delta/\Delta t)$ is the spatially and temporally averaged slip velocity. Consistent with the crack model estimate (8.1a), for the 1968 Saitama, Japan, earthquake the ratio estimated from equation (8.1b) is 11 MPa s/m [*Abe*, 1975]. Similarly for other large earthquakes in Japan, the 1931 Saitama, 1943 Tottori, 1948 Fukui, 1963 Wasaka, and 1968 Saitama earthquakes are consistent with scale independence and a representative value of $\sim 10 \text{ MPa s/m}$ [*Abe*, 1975] (solid line, Figure 8.1b). These data are superimposed as open diamonds on Figure 8.1b along with individual experiments from the Lamont [*Johnson et al.*, 1973], USGS 2 meter [*Beeler et al.*, 2012], and USGS triaxial [*Lockner et al.*, 2010, 2017] testing machines. The lab data are consistent with the earthquake data within reasonable uncertainties. The lower dashed line is a stress drop one half that of the solid line (equation [8.1b]), effectively a Brune model, $\Delta\tau_s = \hat{V}\mu/(2\beta)$ with $\mu/\beta = 10 \text{ MPa s/m}$ [*Brune*, 1970], whereas the upper dashed line is a stress drop twice as large as the solid line. There are deviations from these apparent bounds for the very lowest stress drops in *Beeler et al.* [2012] and largest stress drops of *Lockner et al.* [2010, 2017]; these deviations that are reasonably well understood are discussed in section 8.4.2.

While *Johnson and Scholz* [1976] point out that similar values of the product (8.1a) for earthquakes and for stick-

slip in the Lamont biaxial could be “a fortuitous result of the loading machine design,” the fact that the relationship holds in two other testing machines with fault lengths that vary by more than an order of magnitude suggests instead a robust and useful relationship for relating stick-slip experiments to earthquakes [*McGarr*, 2012]. In any event, the origin of this scale independence of stick-slip properties warrants further investigation and it is the primary motivation for the present study. In this chapter we report the results from stick-slip experiments conducted in a biaxial double direct shear configuration (DDS) [*Dieterich*, 1978]. Stick-slip is documented by directly measuring shear stress drop, fault slip, slip velocity, event duration, and the stiffness of various components of the loading system. The experiments are intended to determine the physical and machine-dependent controls on stick-slip source properties. The focus is on seismically observable quantities and how those values relate to their natural counterparts. The measurements are also used to develop a mechanical model of the experiments. With these new observations of stick-slip source properties and insights on interactions between the source fault and the testing machine, we determine the origin of and limits on the scale independence of stick-slip.

8.2. EXPERIMENTAL PROCEDURES

The experiments were conducted at ambient room temperature and humidity conditions using the DDS test apparatus (Figure 8.2a, b) [*Dieterich*, 1978; *Linker and Dieterich*, 1992; *Kilgore et al.*, 1993, *Kilgore et al.*, 2012] and samples manufactured from Sierra White granite from Raymond, California. The sample geometry is the standard for this apparatus: two smaller side blocks of granite with linear dimensions of $5 \times 5 \times 2 \text{ cm}$ and one larger center block measuring $8 \times 5 \times 4 \text{ cm}$. The two sliding fault areas are each $5 \times 5 \text{ cm}$. A constant normal stress of 2 MPa is maintained by the horizontally aligned hydraulic ram where the output of a load cell is the servo feedback signal. The applied shear force is generated by

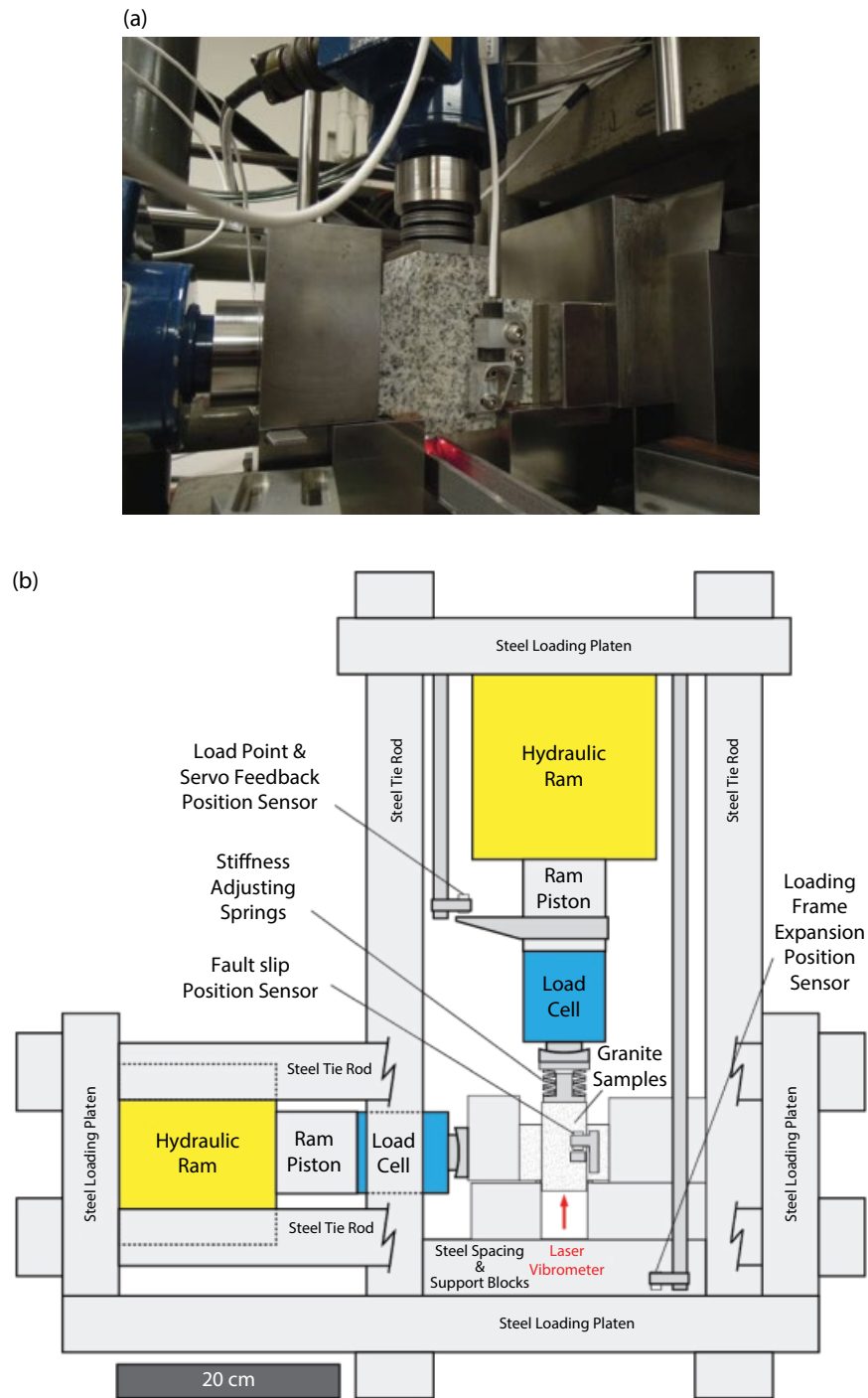


Figure 8.2 Experimental geometry. (a) Photograph of the apparatus. The configuration from left to right is load cell for normal stress, steel spacer block, left stationary sample, center sample, right stationary sample, and steel spacer blocks. The configuration from top to bottom is load cell for shear stress, steel piston, springs, steel spacer, and center sample. The channel structure below the center sample block holds a 45° mirror which directs the laser vibrometer beam to the bottom surface of the sample. The fault displacement sensor in front has a white wire protruding from it. (b) Detailed scale drawing of the apparatus, including the measurement and control points of displacements used to determine the stiffness of the apparatus and fault slip.

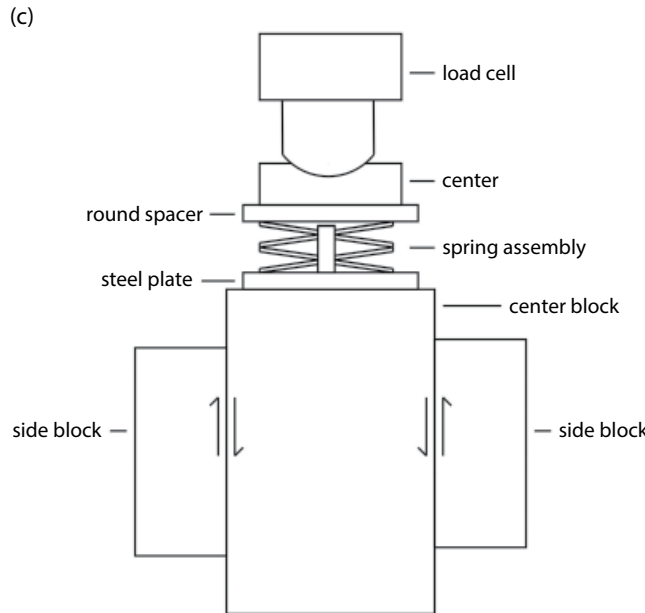


Figure 8.2 (Continued) (c) Sketch of the details of the sample configuration (not to scale).

the vertically aligned hydraulic ram. The position of the shear force piston (located between the hydraulic ram and load cell) relative to the shear-loading frame is the servo feedback signal and the load point for these tests. In all tests, the shear-forcing piston is advanced at a constant rate of $0.2\mu\text{m/sec}$. Position feedback from the load point, rather than force feedback from the load cell, prevented the shear loading servo system from overcompensating after each stick-slip event and, depending on the stiffness, usually allowed the system to complete more than one stick-slip cycle without interruption until the position sensors moved beyond their range and needed to be reset. Examples of complete experiments are found in a Supplement that is available from the corresponding author. A computer control program provided the reference signals for both the normal stress and shear force servo systems.

The fault surfaces are prepared by first machine grinding those surfaces flat with a #100 grit abrasive wheel, then finished by hand lapping the sliding surfaces on dry #600 SiC wet-dry sand paper attached to a glass plate. The fault surfaces are resurfaced with new #600 SiC wet-dry sand paper after each run. The average roughness of the prepared fault surfaces was measured to be approximately $\text{Ra} \leq 0.5$ microns, using a Qualitest TR200 portable surface roughness tester. The flatness and smoothness of the fresh fault surfaces is qualitatively demonstrated by the adhesion between two fault surfaces when those surfaces are pressed together by hand with a twisting motion. The fault surfaces adhere to each other, though with less strength than the bonding observed when machinist's gauge blocks are "wringed" together. After each run, no sliding surface damage or accumulated fault gouge was readily apparent, though a finger swipe revealed the presence of fine fault gouge.

The principal measurements in these tests are shear and normal stress applied to the simulated fault surfaces, fault shear and normal displacement, motion of the shear-loading piston relative to the loading frame, and fault slip rate. To properly document the rapid and transient stick-slip motions in these tests, all the sensors and signal conditioning used in these experiments to document those motions were either selected, or designed and built in the lab, to produce signals with a linear response to 50 kHz or better. The canister load cells measuring the shear and normal stresses applied to the faults are the only exception; they have a resonant frequency of 4 kHz and a linear response below that. All sensor signals were recorded continuously at 500,000 samples per second, averaged on the fly, and data were saved to disk at the rate of 1,000 samples per second. During rapid slip events, all signals were recorded for approximately 0.5 seconds using a pre-trigger/post-trigger transient waveform recorder, saving data to disk at the rate of a million samples per second.

Fault-parallel slip and fault-normal displacement are measured with small eddy-current position sensors mounted within a few millimeters of one of the sliding faults. The proximity of these position sensors to the fault motion minimizes the sensitivity of those measurements to the elastic deformation of the surrounding test apparatus and the granite samples. The motion of the shear and normal stress loading pistons relative to the loading frame, as well as the deformation of the loading frame, were measured using similar position sensors. The velocity of the center sliding sample block during stick-slip was measured directly using a single-point laser vibrometer that is mounted on a tripod with feet that rest

upon small vibration isolation pads on the concrete floor of the laboratory. The floor provides a stable and stationary reference for the velocity measurement. The laser is directed at a 45° mirror that is held by an extending arm attached to the vibrometer itself. The mirror directs the laser to the bottom of the center block, where it reflects back to the mirror and the vibrometer.

The primary goal of these experiments is to determine the dependence of earthquake source properties on the characteristics of the testing machine. This was accomplished by inserting small disc springs between the shear force load cell and the center sample block (Figure 8.2c), which allowed the stiffness of the shear-loading column of the test apparatus to be reduced incrementally. The disc springs were selected with ratings that exceeded the forces applied during the tests, no springs showed any signs of permanent deformation during the tests, and it is assumed that the springs performed within their fully elastic limits. The number and orientation of the disk springs permitted the stiffness of the shear force column to be adjusted over an order of magnitude. The disc springs are not individually calibrated devices, although each has a manufacturer's intended spring constant of about 14 N/ μ m. Friction between stacked springs and between the springs and their mounting device was not accounted for during these tests. Accordingly, shear loading and unloading stiffness was determined empirically in all tests. The loading stiffness was determined from fitting the linear portion of the stress versus load point displacement records during loading (see examples in the Supplement available from the corresponding author). Unloading stiffness was determined using the ratio of the static stress drop to the total event slip, as inferred from the high-speed records (see below).

8.3. RESULTS

Experiments were conducted at eight different values of shear loading stiffness, here and throughout defined as the increment change in shear stress per meter of advancement of the shear load piston. Stiffness was varied between approximately 0.92 and 23.3 GPa/m, and between 6 and 16 stick-slip events were recorded for each stiffness. The summary values of number of events, slip, slip velocity, static stress drop, stiffness, and their measurement uncertainties are listed in Table 8.2. Figure 8.3 shows two representative examples of the scaled data from slip events at the highest (Figure 8.3a) and lowest (Figure 8.3b) stiffnesses. The horizontal axis is time and both events are shown at the same total scale (0.0017 s). The vertical stress axis is the same for both events while the velocity and slip have different scales for each event. At high stiffness (Figure 8.3a) stress drop, slip and slip velocity are relatively small. Event duration is also much shorter than at low stiffness.

In detail, the velocity record at high stiffness is complex, showing three local maxima. These may be related to slip on the two parallel faults in the DDS geometry not being exactly coincident in time. However, at low stiffness, ignoring the small-amplitude high-frequency oscillation (Figure 8.3b), the velocity-time history is so simple as to be well represented by a sine function, similar to the study by *Johnson and Scholz* [1976]. There are complications in the stress measurements. For both events shown, and as is typical throughout this suite of experiments, the normal stress is not exactly constant over the slip event. Apparently, vibrations produced by rapid slip have shorter periods than the response time of the fault normal servo-control system. These vibrations are larger and have longer periods for the larger stress drop at low stiffness, but we do not find that these normal stress artifacts affect any of the conclusions of this study. At low stiffness where the slip speeds are the largest, the shear stress record shows a systematic oscillation with a period around 0.00016 seconds (Figure 8.3b). This is of the order of the resonance frequency of the load cell (4 kHz) and is likely to be related to the instrument rather than the fault behavior. Although this is not ideal, for all events at all stiffness we use the initial and final values of the load cell measured stress to determine stress drop, in other words, the static stress drop, and so we believe that the oscillations do not affect any of the conclusions of this study.

As seen in Figure 8.3b, for the stick-slip generated by the least stiff shear loading column, the shear stress dropped more or less gradually to a new static level. For the stick-slip generated by the most stiff shear loading column (Figure 8.3a), the shear stress drop displays an apparent rapid stress overshoot, followed by recovery to a new static stress level. The duration of the rapid shear stress drop in the events with the stiffest shear loading column unfortunately coincides with the resonant period of the load cell, and since the stress recovery following the overshoot occurs after slip has stopped, it is unclear whether the overshoot is real or instrument resonance. Improved measuring stress techniques are planned for future work to resolve this issue. While the static stress drop is used to estimate the unloading stiffness, this apparent overshoot is a relatively small fraction of the static stress drop, and the uncertainty associated with the apparent overshoot also does not effect the overall conclusions of this study. That is because this is a study of scaling; the eventual scaling relations presented below are power law, and even first-order measurement errors do not have a significant impact (see Figure 8.5 and associated discussion).

For most stick-slip events (see Figure 8.3), the onset of slip was characterized by an emergent signal from the fault slip sensor. The emerging slip signal is likely caused by a combination of accelerating fault creep and a small

Table 8.2 Stick-slip of granite at 2 MPa normal stress, 0.2 $\mu\text{m}/\text{s}$ loading rate, and variable stiffness.

N	Δt_{obs} (μs)	$\Delta\delta$ (μm)	V (m/s)	V_{peak} (mm/s)	$\Delta\tau_s$ (MPa)	k_{load} (MPa/m)	k_{unload} (MPa/m)	Spring Assembly Mass (kg)	Total Mass (kg)	Loading $k\Delta t$ (MPas/m)	Unloading $k\Delta t$ (MPas/m)
6	1095.7 ± 21.1	816.4 ± 157	0.7451	1064.4 ± 185.9	0.744 ± 0.101	977.5 ± 147.1	922.3 ± 85.2	0.1412	0.6472	1.071	1.011
11	759.3 ± 32.2	293.8 ± 29.5	0.3869	628.9 ± 35.2	0.5031 ± 0.0348	1570.9 ± 105.6	1719.1 ± 83.1	0.0954	0.6008	1.193	1.305
15	908.3 ± 7.3	192.1 ± 18.5	0.2115	345.6 ± 31	0.5108 ± 0.0398	2473.2 ± 76.9	2664.7 ± 77.4	0.0478	0.5532	2.246	2.420
11	560.6 ± 34.6	47.1 ± 11.6	0.08402	131.5 ± 25.8	0.209 ± 0.055	4522.5 ± 341.9	4428.3 ± 394	0.0305	0.5359	2.535	2.483
16	329.1 ± 8.2	18 ± 0.7	0.05469	106.4 ± 1.8	0.264 ± 0.019	15319 ± 622.5	14673 ± 624	0.0478	0.5532	5.042	4.829
11	359.2 ± 14.1	51.6 ± 2.4	0.1437	215.7 ± 10	0.514 ± 0.038	9267.7 ± 416	9267.7 ± 416	0.0689	0.5743	3.329	3.329
16	257.3 ± 5	12.9 ± 0.2	0.05014	89.6 ± 2.3	0.277 ± 0.018	20876 ± 153	21538 ± 1594	0.0911	0.5965	5.372	5.542
15	281.7 ± 8.8	10.7 ± 0.4	0.03798	78 ± 3.2	0.25 ± 0.004	20323 ± 207.1	23308 ± 893	0.133	0.6384	5.725	6.566

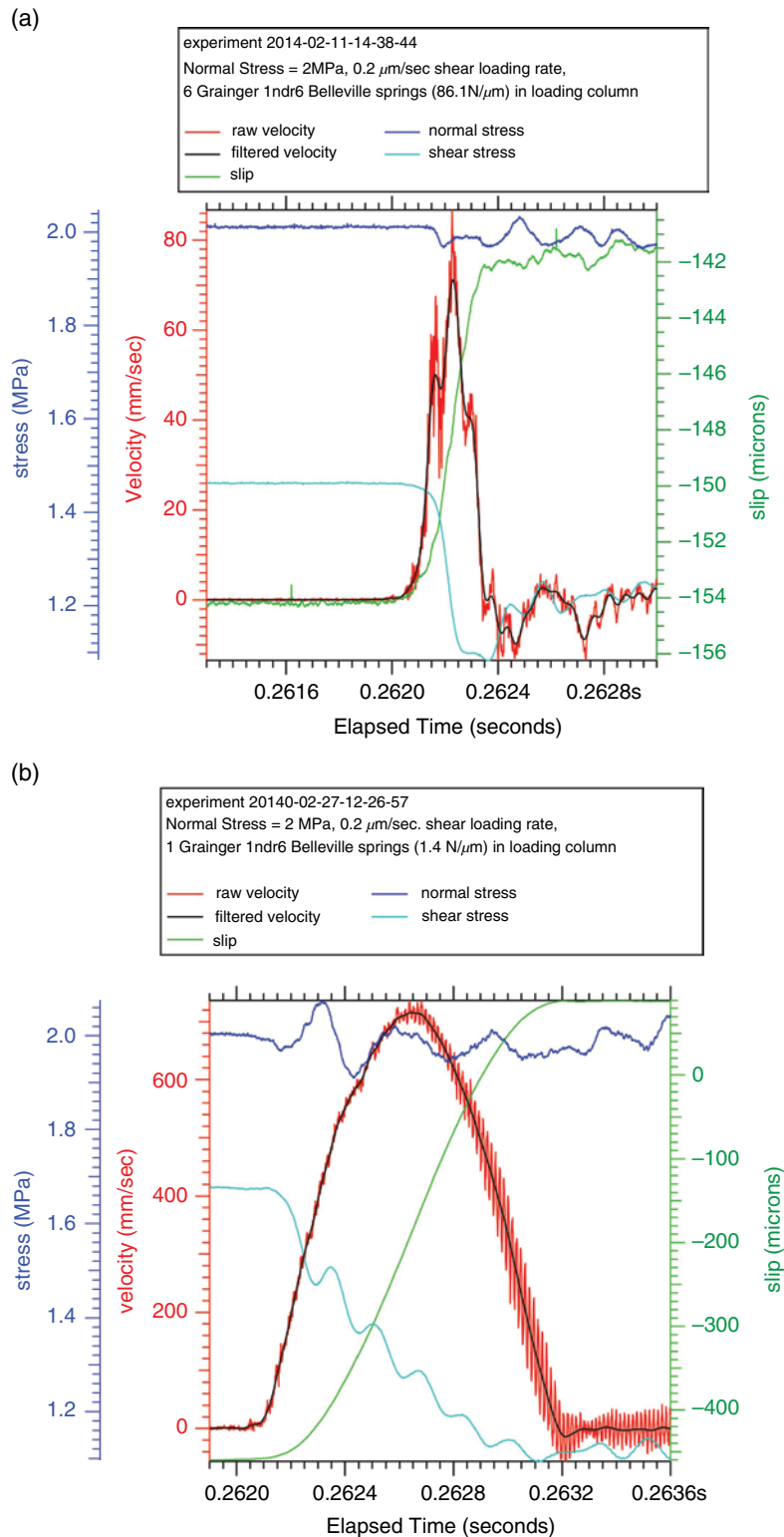


Figure 8.3 Stress, slip, and slip velocity during slip events at high and low stiffness. (a) Data at unloading stiffness of 23 GPa/meter. (b) Data at unloading stiffness of 0.9 GPa/meter.

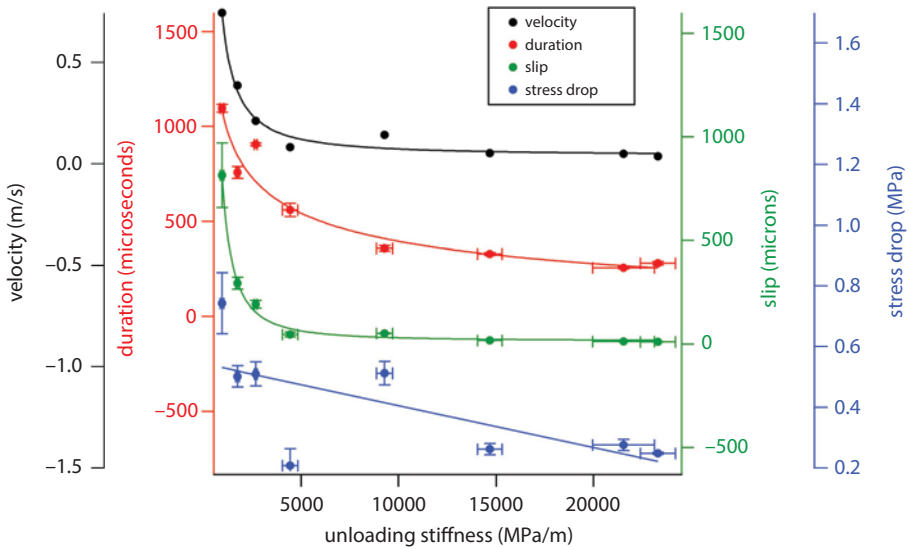


Figure 8.4 Duration, average slip velocity, slip, and stress drop with unloading stiffness. Error bars indicate \pm one standard deviation. Data are listed in Table 8.1.

component of elastic shear deformation of the sample between the mounting points of the fault slip sensor on each side of the fault. In contrast, the slip velocity of the center sliding block, measured by the laser vibrometer, revealed a more abrupt onset of fault motion. We use the abrupt acceleration of fault slip from the velocity records to determine the start of fault slip and the subsequent zero crossing of the velocity record to determine the end of fault slip. Those same start and end picks were also used to determine event duration.

The average velocity is the ratio of total slip to duration while the peak velocity was measured directly by the laser vibrometer. A simple integration of the observed slip velocity (not shown) produces a slip record that closely matches the observed slip record, demonstrating the validity and self-consistency of the separate velocity and slip measurements. The unloading stiffness is the ratio of the static stress drop to the total slip while the loading stiffness was determined by measuring the stress change on the loading column per increment of loading displacement over much of the shear loading portion of each stick-slip cycle. The loading and unloading stiffnesses are similar, as expected (Table 8.2). The results for all events at each stiffness were averaged, and the resulting values and associated standard deviations of the measurements are tabulated in Table 8.2. The average values of slip, duration, slip velocity, and stress drop with unloading stiffness are also shown in Figure 8.4.

Decreasing stiffness by a factor of 25 increases slip event and slip velocity. Slip increases monotonically by 74 times from 11 to 816 microns, and average slip rate increases by 19 times from 0.04 to 0.74 m/s, also following a well-constrained trend. It is worth noting that these

systematic changes in slip rate differ from earthquake scaling; as typically reported, slip rate is independent of rupture dimension, i.e., stiffness. A decrease in duration is similarly well defined, but the variation is much weaker than for slip and velocity, changing by 3.9 times from 1.1 to 0.28 ms. In contrast to total slip, average slip velocity, and duration, there is no systematic dependence of static stress drop on stiffness. There is a net decrease from 0.74 to 0.25 MPa, but this is a factor of only 3. The weak relationship is perhaps complicated by the tests at unloading stiffness of ~ 9.3 GPa/m that show a high stress drop relative to the trend from the other tests. However, we have no reason to exclude this result and conclude that these preliminary tests show no clear dependence of stress drop on stiffness.

These above-described relations between stiffness, slip, duration, slip velocity, and stress shown in Figure 8.4 are the new experimental observations of possible stick-slip scaling from this study. A summary of the dependences of slip, duration, and slip velocity on the imposed changes in stiffness are indicated by the curves superimposed on Figure 8.4; these are fits to the data with a power law that captures the relationships. Thus, the qualitative interpretation is that all of these quantities depend nonlinearly on stiffness. In contrast, the dependence of stress drop on changes in stiffness is unclear. The linear relation fit to the stress drop data shown in Figure 8.4 (open diamonds) is a poor representation, even given the uncertainty of the measurements. That is, the dependence of stress drop on machine stiffness is not resolved by this dataset. The variability seen between data at different stiffnesses may reflect actual variations of the physical properties of the fault surface.

8.4. INTERPRETATION AND SCALING RELATIONS FROM STICK-SLIP

The systematic relationships between stiffness, duration, stress drop, and slip rate in this dataset do not follow the expected scaling of earthquakes seen in previous stick-slip studies as compiled in Figure 8.1 and as suggested by *McGarr* [2012]. In the following section, we develop explanations for the scaling relationships depicted in Figure 8.5. Analysis relating laboratory stick-slip to natural earthquakes is found in the subsequent section (8.4.2) below.

8.4.1. Slider Block Model

The systematic relationships in this dataset closely follow expectations from modeling the fault and testing machine as a slider-block [*Johnson and Scholz*, 1976; *Rice and Tse*, 1986]. Accordingly, the duration of a slip event, Δt , is half the resonance period of the machine, T , and is inversely proportional to the square root of the system stiffness. In the case of undamped motion the relation is

$$\Delta t = \pi \sqrt{\frac{m}{Ak}}, \quad (8.2a)$$

where m is mass and A is fault area [*Johnson and Scholz*, 1976; *Rice and Tse*, 1986]. In the test configuration (Figure 8.2b), the compliant disc springs are below the end of the shear loading piston and immediately above the center fault block. The rest of the testing machine above the springs, including the piston, load cell, platen, and frame is much stiffer and can be treated as stationary. The two side fault blocks are stationary, so the “fault” consists only of the center block and the spring assembly, consisting of the springs and a center post and screw. The mass of the spring assembly varies between tests at different stiffnesses, while the center block has a mass of $\sim 0.432\text{ kg}$, resulting in variations in fault mass of up to 21% (Table 8.2). Measured duration from the experiments is shown as the black dots on the log log plot of duration versus stiffness in Figure 8.5a. Predicted duration from equation (8.2a) based on the known mass, the area of both faults in the DDS geometry, and unloading stiffness is shown by the open diamonds. A fit to those predictions with equation (8.2a) is shown as a dashed line. The prediction, based on a model with no free parameters, matches the observations to within the data uncertainties. Two other fits to the observations are also shown. The first empirically uses the form of equation (8.2a) where duration varies inversely with the square root of stiffness, treating the constants such as mass, fault area as a single free parameter (black dashed line). The second is the power law fit first shown in Figure 8.4 (in Figure 8.5a, it is the

black solid line). The slope of the power law fit is -0.46 , very close to the expected -0.5 from equation (8.2a). From this analysis we conclude that the weak systematic dependence of duration on stiffness (Figure 8.4) likely is independent of the frictional properties of the fault (stress drop) and is imposed by the nature of the testing machine-fault interaction.

Although the predicted and observed durations agree to within the data uncertainty, the respective fits with equation (8.2a) (dashed lines) are slightly offset. An apparent offset of this sense, while not resolved in these experiments, is expected due to radiation losses or fracture energy not accounted for in equation (8.2a). The appendix develops an approach for estimating apparent stress, radiated energy and overshoot, based on this offset. Nonetheless, because of the offset we use the empirical data fit (solid line, Figure 8.5a) to illustrate other predictions from the slider block model that are consistent with the systematic variation of slip velocity and slip with stiffness, as follows. For slip velocity, the average velocity is $\hat{V} = \Delta\delta/\Delta\tau$. As the stiffness is $k = \Delta\tau_s/\Delta\delta$, the expected relation between velocity and stiffness for undamped motion is

$$\hat{V} = \frac{\Delta\tau_s}{\pi} \sqrt{\frac{A}{mk}}. \quad (8.2b)$$

In this case the relationship involves the fault properties via the stress drop, as well as a dependence on stiffness from the testing machine. In any event the prediction (8.2b) (Figure 8.5b, dashed line) matches the observations and differs little from a fit of a power law to the data (black line). Note here that the prediction in Figure 8.5b is not a fit to the data with the power law exponent fixed at 1. Rather, it is the prediction of the spring slider relation (8.2b) using the coefficient $10^{-1.43}$ from the fit of that equation to the duration and stiffness data shown in Figure 8.5a (dashed line). The expected total slip resulting from undamped motion is

$$\Delta\delta = \pi \hat{V} \sqrt{\frac{m}{Ak}}. \quad (8.2c)$$

Again, the prediction from the model (dashed line, Figure 8.5c) is consistent with the observations and is nearly identical to an unconstrained power law fit to the data.

8.4.2. Relationships Between Stick-Slip and Earthquake Source Properties

Since scaling of duration with stiffness in these experiments follows a slider-block model, the experiments do not conform to *McGarr’s* [2012] hypothesis (Figure 8.6a) and cannot be directly scaled to natural earthquakes.

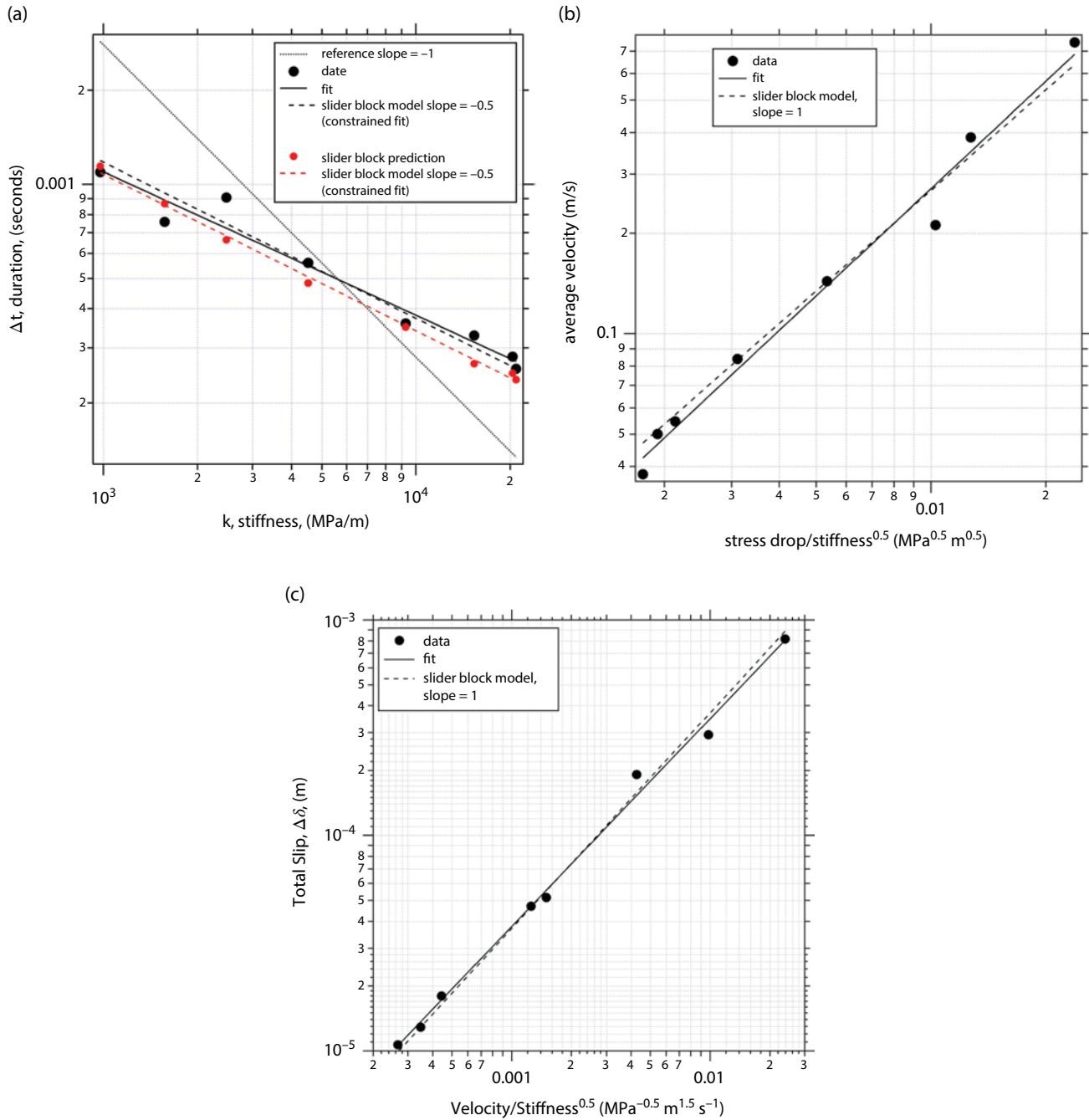


Figure 8.5 Comparisons between data and predictions from a slider block model. (a) Duration versus stiffness. Open diamonds are the predictions of equation (8.2a) for duration from the known fault mass, stiffness, and area (Table 8.2). The dashed line is a constrained fit to these predictions with $n = -1$. Black dots are the observed durations. The black solid line is a fit of these data to a power law $y = Cx^n$, where $C = 10^{-1.58}$, $n = -0.46$. The black dashed line is a constrained fit with $n = -0.5$, resulting in $C = 10^{-1.43}$. The dotted line is a reference line for an inverse proportionality between duration and stiffness, a constrained fit to the data with $n = -1$. (b) Average sliding velocity versus stress drop/(stiffness^{0.5}). The solid line is a fit resulting in $n = 1.07$. The dashed line is a prediction from the power law relation equation (8.2b) using the appropriate coefficient from the fit shown in (a) ($10^{1.43}$). (c) Total slip versus average velocity/sqrt(stiffness). The solid line is a fit resulting in $n = 0.96$. The dashed line is a prediction from the power law relation equation (8.2c) using the coefficient from the fit shown in (a).

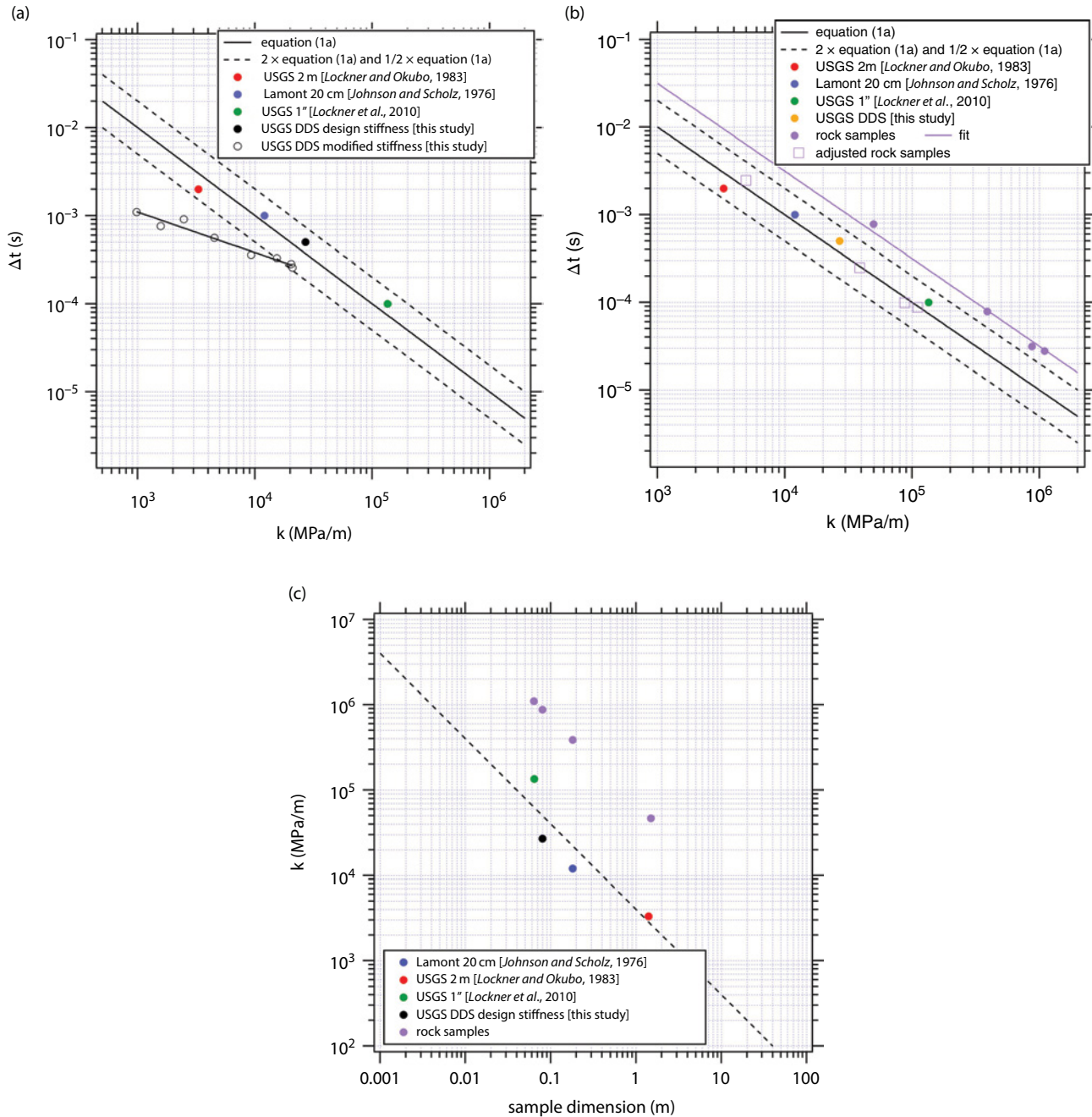


Figure 8.6 Earthquake source properties from stick-slip. (a) Duration versus stiffness as shown in Figure 8.1a with the addition of the design stiffness and observed duration of stick-slip in the USGS double direct shear (DDS) machine (solid triangles), and the results from the same machine with its stiffness systematically reduced (open black circles). The solid line is the scale-independent prediction, equation (8.1a) with $\mu/\beta=10\text{ MPa s/m}$, and the two dashed lines are one half and two times equation (8.1a). (b) Duration versus stiffness as shown in part (a) for the four testing machines. X's are estimated durations assuming the rock samples of the four testing machines are the most compliant element in the system (see text). Dash-dotted line is a constrained fit to an inverse proportionality resulting $k\Delta t=31\text{ MPa s/m}$. The +'s squares result from reducing the stiffness ten times less than that of the rock samples (see text). (c) Stiffness versus sample dimension for the four testing machines. The dashed line is an inverse scaling relationship that suggests apparatus stiffness is approximately inversely proportional to sample size for these machines collectively. Shown for reference is the estimated stiffness of the rock samples, which is calculated from the sample dimension in Table 8.1 and an assumed modulus (see text for discussion).

Furthermore, while slip decreases with stiffness as it does for natural earthquakes, the dependences of duration and slip velocity on stiffness are inconsistent with results for earthquakes. Despite these complications, there may be some value in these measurements. In particular, the static stress drops in this study are in the range of 0.25 to 0.74 MPa, within the bounds, but in the lower range observed for natural earthquakes [Baltay *et al.*, 2010, 2011] probably owing to the low normal stress (2 MPa). The lack of a strong or systematic dependence of stress drop on stiffness is also consistent with the natural observations. Nevertheless, given the expected and observed normal stress dependence of stress drop [e.g., Lockner *et al.*, 2017], the resemblance with natural stress drops may be fortuitous. Similarly, the estimate of apparent stress in the appendix is consistent with earthquakes, but it is unclear whether this is a coincidence. In prior studies of rapid slip with a slider-block model [e.g., Beeler, 2001] the ratio of apparent stress to stress drop for stick-slip is fixed at about 0.25, which agrees well with the 0.22 as estimated in the appendix. These values are not unlike standard earthquake models [e.g., Brune, 1970; Singh and Ordaz, 1994] and are consistent with natural observations [Baltay *et al.*, 2011]. Unfortunately, the estimated average ratio of apparent stress to stress drop determined from the data, 0.22, is not well constrained by the observations, and it is unknown to what degree this measure of efficiency is influenced by the properties of the machine; slip during unconfined rupture in most test geometries is mechanically constrained to overshoot.

Despite these questions concerning relevance to earthquakes, in the next few paragraphs we develop a broader view of scaling of stick-slip by considering the procedures used in the experiments, the unaltered properties of all the testing machines shown in Figure 8.1, and the properties of the DDS apparatus. This analysis is qualitative in nature but is strongly supported by the empirical data, leading to a more optimistic perspective on the value of stick-slip to understanding the earthquake source and additional support for McGarr's [2012] hypothesis. Experiments conducted at the unaltered machine stiffness of the DDS apparatus 27 GPa/m (Table 8.1), result in a measured duration of ~ 0.0005 s. These values plot well within bounds of the prior studies (Figure 8.6a), and the product of stiffness and duration is 13.5 MPa s/m, of the same order as in the other testing machines. So, while the duration and stiffness from the primary experiments plot well off trend from the results of prior studies (Figure 8.6a) and earthquakes (Figure 8.1a), this seems to result entirely from the testing procedure where the stiffness is reduced. A simple view, which we will expand upon momentarily, is that the relationships between stiffness and duration (Figure 8.5a), stress drop and loading velocity (Figure 8.5b), and slip

and slip velocity (Figure 8.5c) are "artificial" due to the stiffness being changed, independent of the scale of the fault. Implicit in this interpretation, which we will also expand upon momentarily, is that the scaling of earthquake source properties, such as between stress drop and slip speed, can only be inferred from stick-slip experiments in a single machine when the stiffness is constant at the design value and stress drop varies significantly (Figure 8.1b). Similarly, the relation between duration and stiffness can only be inferred from comparing values between machines (Figures 8.1a and 8.6b), where stiffness and scale are apparently interdependent in the same way as for earthquakes.

Throughout the remaining discussion, we use the adjectives *design* or *natural* to refer to the stiffness or stick-slip duration that results when these various rock testing apparatuses are used as intended by their designers and manufacturers. These adjectives should not be interpreted to imply that resulting stiffness or stick-slip duration was intended to produce realistic earthquake source properties. On the contrary, as described below, our conclusion is that realistic and scale-dependent earthquake source properties result during stick-slip largely as a consequence of using rock samples with the same elastic properties as the earth and from consistent but unintentional design practices that are themselves scale-independent.

McGarr's [2012] hypothesis requires both that the product $k\Delta t$ is scale independent in experiments, as it is for earthquakes, and that the product is of the same order as for earthquakes. How these requirements are met in practice, apparently fortuitously [Johnson and Scholz, 1976], can be understood qualitatively by further examining constraints of the particular experimental geometries, noting the mechanical requirements for stick-slip, and by considering the intended purpose of the various testing machines. While a detailed mechanical analysis of the four individual machines is beyond the scope of the present study, the scale independent $k\Delta t$ arises primarily from basic requirements of doing faulting tests at different scales. For example, even though there are four different machines and three different fault geometries (direct shear, double direct shear, and triaxial), collectively the rock sample masses, fault areas, and characteristic dimensions L (Table 8.1) conform to the requirements of $k\Delta t$ being scale independent. That is, we assume the rock sample is the most compliant element in each of the four machines. Then, taking the loading stiffness to be E/L , $\rho = 2700 \text{ kg/m}^3$ and $E = 70 \text{ GPa}$ results in the durations calculated from equation (8.2a) shown as X's in Figure 8.6b. The product of the sample stiffness and this duration is included in Table 8.1 as the "estimated sample $k\Delta t$." A power law fit to these sample-inferred duration and stiffness produces a slope of -1.08 , very close to the inverse proportionality. A constrained fit for

the inverse proportionality results in the product being 31 MPa s/m (dash-dotted line), only a factor of three larger than the ~10 MPa s/m, appropriate for earthquakes and the representative value for the testing machines. That stick-slip is not possible if the rock samples provide all of the system compliance is a rationale for why the testing machines that are capable of producing stick-slip have a smaller stiffness, larger duration, and smaller product than the samples they load. A comparison of the sample stiffness to the stiffness of the testing machines and how these stiffnesses scale with sample dimension is shown in Figure 8.6c.

In the case of the triaxial and DDS configurations, these machines were intended to be primarily used for stable frictional sliding, rather than stick-slip, and indeed their loading frames are quite stiff. For example, *Lockner et al.* [2017] find that about two thirds of the compliance of the triaxial is from the sample itself and one third from the apparatus (Figure 8.6c). Stick-slip can be accessed in these stiff machines in their design configuration by conducting experiments at high normal stress in triaxial [*Lockner et al.*, 2017] or in DDS experiments using faults with highly polished surfaces [*Dieterich, 1978*]. Similarly, though the Lamont and 2 meter biaxial machines were intended for rupture propagation and stick-slip, they are not highly compliant relative to the others once the differences in scale are accounted for. Although there is scatter in the scaling relation (Figure 8.6c), the dashed line indicates an inverse proportionality. Based on this plot we conclude that even though the intended purpose of these testing apparatuses was not for stick-slip in all cases, their stiffnesses scale approximately inversely with the size of the samples; furthermore, the scaling is in part just a requirement of conducting experiments on different-sized samples. This scaling can be rationalized by noting that all designs consist of similar components (platens, tie bars, pistons, hydraulics) of the same composition (steel, hydraulic oil). Likely, the relatively tight scaling is also influenced by design practice requirements for the relatively compliant machines to nonetheless have fairly high stiffness to reduce long period vibrations, and to minimize bending and stored elastic energy for performance and safety considerations.

Returning to the scaling of duration and stiffness estimated from the four samples (Figure 8.6b, X's), since the requirement for stick-slip is more compliance than the rock samples and the time constant goes as $1/\sqrt{k}$, a reduction in stiffness increases the time constant. The net effect is a smaller reduction in the $k\Delta t$ than in the stiffness. So, for example, a 10x reduction from the stiffness of the rock samples produces an approximate 3x increase in duration and 3x reduction in the product (Figure 8.6b, +'s). While the shift from the sample stiffness and duration in this simple calculation is not an exact match for all four of the

machines, a 10x reduction in stiffness produces overall shifts of the duration and the product that are consistent with the collective observations.

8.5. LIMITATIONS, CONSTRAINTS ON LAB-INFERRED SOURCE PROPERTIES, AND CAUTION

Significant experimental limitations on the data from this study include the measurement problems associated with shear stress measured at the load cell (Figure 8.3b). This issue may be resolved by replacing the present load cell with an instrument with a higher resonance frequency. Direct measurement of on-fault shear resistance using strain gauges and also employing a near fault thermocouple that could be used to determine the average shear resistance should complete energy accounting during stick-slip and provide measurement redundancy. It would be ideal to measure radiated displacements directly and to determine radiated energy for comparison with calculations described in the appendix. Complications include small sample dimensions relative to the normal and shear loading column lengths, which lead to returning reflected waves from the piston-sample interface that are nearly instantaneous relative to the total duration of fault slip if the measurements are made on the rock samples. Nevertheless, the calibration approach described by *McLaskey et al.* [2015] may be suitable for this kind of accounting.

The experiments in this study were intentionally limited to a single normal stress and loading rate to focus on mechanical interactions between the fault and the testing machine. Experiments over a range of normal stresses are necessary to fully relate stick-slip results to natural seismogenic depths. The 2 MPa normal stress in the present tests correspond to a depth of a few hundred meters in the Earth, whereas, for example, the effective normal stress at the base of the seismogenic zone on the San Andreas may be roughly 100 times higher. Experiments with variations in loading rate and experiments at the same stressing rate are also needed for a more complete study of stick-slip source properties. The extrapolation to the Earth entails much lower stressing rates than in the present suite of experiments. The lowest stressing rate in our experiments is about 5.8 GPa/yr compared with tenths or hundredths of an MPa/year for natural M6 and larger earthquakes. Unfortunately, experimental difficulties arise in the unconfined double direct shear geometry at higher normal stress. To increase the normal stress significantly requires a larger testing machine or a different geometry. Similarly, since our double direct shear apparatus lacks confinement, such as in the triaxial experiments in Figure 8.1 [*Lockner et al.*, 2010, 2017], tests at elevated

temperature and pore pressure would allow more confident application to natural faulting.

Since reducing the machine stiffness in the DDS apparatus produces stick-slip source properties that scale differently from the natural counterparts (Figure 8.6a), the source properties stress drop, duration, slip, and slip speed from high-speed laboratory faulting and stick-slip are only directly relevant to natural earthquakes under limited conditions. The bounds depicted in Figures 8.6 and 8.7 are necessary requirements for earthquake-like source properties, namely, that the product of stiffness and duration, equivalently the quotient of static stress drop and sliding speed, lies between 5 and 20 MPa s/m. In reference to values well outside those bounds, as shown in Figure 8.7, these are offered here as examples of interesting experiments that may not be directly relevant to typical natural earthquakes. The very lowest stress drops

in the *Beeler et al.* [2012] study (Figure 8.7) lie to the left of the bounds and therefore are “slow” relative to earthquakes. As described in more detail in the original study, these tests are conducted at the lowest normal stresses on a fault with high fracture energy. The fracture energy reduces the slip speed, and these events would be faster and have shorter durations were slip not damped by this dissipation. These may be relatable to “low-frequency earthquakes” [Shelly et al., 2006], events that have both lower rupture propagation rates and slip speeds when compared with typical earthquakes with the same moment. Fracture energy is not accounted for in equations (8.1) or (8.2).

At the other extreme are the largest stress drops of the *Lockner et al.* [2010] study (black solid circles). These also plot to the left of the bound and are slower than earthquakes of equivalent stress drop, despite having inferred

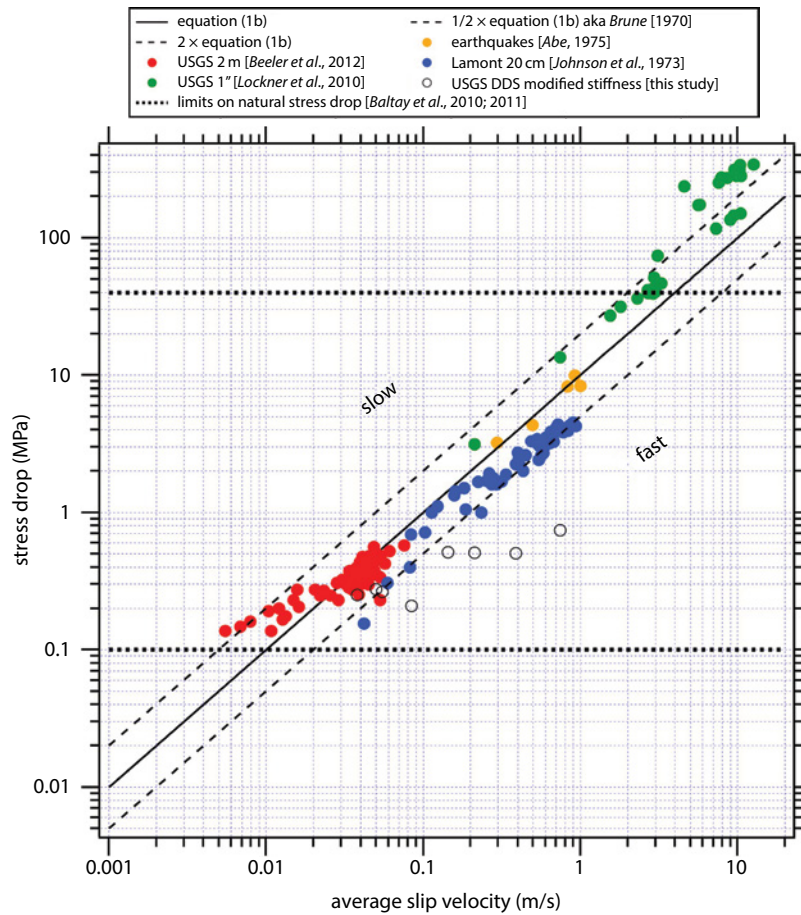


Figure 8.7 Scaling of earthquake source properties from laboratory stick-slip. Static stress drop versus average slip velocity. Data for individual stick-slip events from this study (open circles) are shown along with the prior studies in three different testing machines [Johnson et al., 1973; Beeler et al., 2012; Lockner et al., 2017] and from five Japanese earthquakes [Abe, 1975]. The solid line is the scale-independent prediction, equation (1a) with the impedance $\mu/\beta = 10 \text{ MPa s/m}$, and the two dashed lines are one half and two times (1a). The horizontal dotted lines demarcate the range of typical natural stress drops (0.1 to 40 MPa) inferred from recent analysis using a *Brune* [1970] source model [Baltay et al., 2010; 2011].

slip speeds in excess of 4 m/s. The origin of the damping of slip for these events is not yet completely understood. These produce enough shear heat to melt the fault zone, at least in part, and it is possible that there is dissipation associated with the generation or subsequent freezing of the shear melt that reduces the sliding speed [e.g., *Koizumi et al.*, 2004]. Could this be shown definitively it may provide a signature frequency content of natural melt-generating earthquakes. However, another possibility is that the slow slip is due to contributions from the testing machine. These tests are at the highest confining pressures in the *Lockner et al.* [2010; 2017] study. The confining fluid is a silicone oil whose viscosity increases with pressure and may contribute to slowing the slip rate at high confining pressure. Further limits on the relevance of laboratory-inferred fault properties come from typical earthquake stress drops that are in the range of 0.1 to 40 MPa [*Baltay et al.*, 2010; 2011] (heavy dotted horizontal lines, Figure 8.7). These imply limits on average slip speed of 0.005 to 8 m/s. Both the upper limit on stress drop and slip speed are exceeded in the *Lockner et al.* [2010] experiments at the highest confining pressures. Explaining those differences and other implied differences between laboratory stress drops and earthquakes [e.g., *Di Toro et al.*, 2011] is beyond the scope of the present study but is an important remaining challenge for the experimental fault mechanics community.

8.6. SUMMARY AND CONCLUSIONS

Laboratory stick-slip in standard direct shear, triaxial, and double direct shear testing configurations have effectively scale-independent values of the ratio of static stress drop to average slip rate, between 5 and 20 MPa s/m, so long as the experiments are conducted on rock and at the design elastic properties of the testing machine. The ratio is essentially the same as found for natural earthquakes and, as in seismic source theory [e.g., *Brune*, 1970], is of the same order as the impedance, the ratio of the elastic modulus to the wave speed; the ratio is also equal to the product of the stiffness and the rise time. Collectively, these results confirm the hypothesis of *McGarr* [2012] that the product of stiffness and rise time for stick-slip is scale independent and the same as for earthquakes. The constant ratio arises because the square root of the ratio of the product of sample mass and stiffness to fault area of experimental samples is independent of scale, the apparatus stiffnesses vary inversely with sample size, and the stiffness of the testing machines is approximately ten times smaller than that of the rock samples. Expected and documented exceptions to this rule are cases where fault slip is damped by fault properties (or machine effects), producing events that have lower slip rates than their natural counterparts of equivalent stress drop, and

cases where the testing machine stiffness is reduced from the design values, resulting in larger slip rates than for natural earthquakes of the same stress drop.

ACKNOWLEDGMENTS

Greg McLaskey of the USGS provided a review that significantly improved the manuscript. Monograph reviews by Nicolas Brantut and Chris Marone are gratefully acknowledged. Any use of trade, firm, or product names is for descriptive purposes only and does not imply endorsement by the U.S. Government.

APPENDIX

Estimating Radiated Energy During Stick-Slip

In our experiments radiated energy is not directly measured using high-frequency seismic instrumentation; nonetheless, it might be reliably estimated from slip velocity measurements under some circumstances. For fixed fault area the amount of energy available to be radiated as shear waves due to fault slip is

$$E_{nf} = \frac{A\zeta}{2} \int_0^{\Delta t} V^2 dt \quad (8.A1a)$$

[e.g., *Kanamori*, 2001], where ζ is the impedance. For a fault in an elastic continuum, $\zeta = \mu/\beta$. As pointed out by *McGarr and Fletcher* [2001], for an earthquake, some of this available energy (8.A1a) remains in the near-field and goes into producing the static elastic distortions about the rupture. Laboratory experiments typically lack such a near-field reduction of equation (8.A1a) because spatially uniform slip on the fault nearly always results once rupture reaches the free surfaces at the fault ends, and there is no increase in near-field static strain energy. Therefore, arguably, $E_r = E_{nf}$ and the radiated energy during stick-slip is given by (A1a). Accordingly, all that is needed to estimate radiated energy is the slip velocity. As the apparent stress relates to radiated energy as $\tau_a = E_r / A\Delta\delta$, then

$$\tau_a = \frac{\zeta}{2\Delta d} \int_0^{\Delta t} V^2 dt. \quad (8.A1b)$$

Equation (A1b) for apparent stress is consistent with continuum and slider block models that are radiation damped [*Rice*, 1993; *Beeler*, 2001]. However, for our stick-slip experiments the elastic impedance is constrained by the observations to be much less than μ/β . For example, assuming constant slip rate at the average velocity, the apparent stress in (A1b) becomes $\tau_a = \frac{\zeta \hat{V}}{2}$; taking the impedance to be 10 MPa s/m and the average

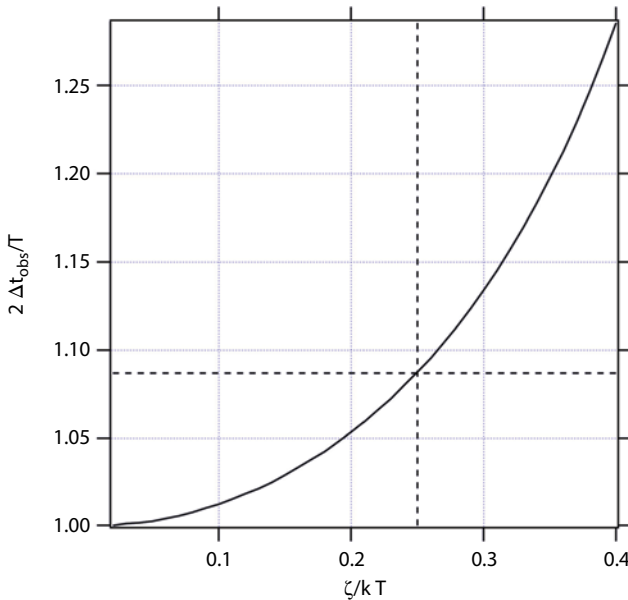


Figure 8.A1 Relative increase in event duration with impedance in a slider block model.

slip rate from the lowest stiffness tests, ~ 0.75 m/s, apparent stress would be 3.75 MPa, an order of magnitude larger than the stress drop and higher than the normal stress on the fault. This is a physically impossible value for apparent stress.

A more appropriate estimate for the impedance can be made using a slider block model that accounts for radiation loss [Beeler, 2001]. The idea is to attribute to radiation loss the difference between the observed event durations and those inferred using the undamped slider block model, equation (8.2a) (Figure 8.5a, Table 8.2). For a static-kinetic fault strength relation with dynamic stress drop $\Delta\tau_d$ and a single degree of freedom spring-slider block model, the equation of motion is the balance of the mass times acceleration against the difference between the spring force and the frictional resisting stress, less the radiated energy:

$$\left(\frac{T}{2\pi}\right)^2 \frac{\partial^2 \delta}{\partial t^2} = \frac{\Delta\tau_d}{k} - \delta - \frac{\zeta}{2k} \frac{\partial \delta}{\partial t}. \quad (8.A2a)$$

T is the undamped characteristic oscillation period, and the event duration in the absence of radiation is $\Delta t = T/2$. k is stiffness, ζ is impedance, and δ is slip on the fault. The third term on the right-hand side of (A2a) is the “radiation damping” term, used to approximate energy lost as propagating seismic waves, here assumed to be planar shear waves [Rice, 1993]. The observed event duration Δt_{obs} is larger than Δt when radiation losses are significant. That condition is met when the impedance is a significant fraction of the characteristic impedance kT of

the undamped spring slider. Averaging the slip velocity over an entire event produces a stress measure of the radiated energy, the apparent stress

$$\tau_a = \frac{\zeta \hat{V}}{2}. \quad (8.A2b)$$

To estimate radiated energy and apparent stress, equation (8.A2a) is solved numerically for slip, stress, and slip rate with time for a range of values for the impedance, representing possible amounts of radiation loss, for comparison with the experiments. Figure 8.A1 shows the ratio of observed duration normalized by the characteristic duration $\Delta t_{obs}/0.5T$ resulting from a range of impedances from zero to 40% kT . To apply these simulations to the observations shown in Figure 8.5a, the experiments are treated collectively by interpreting radiation loss as the difference between the observed event durations and those inferred using the undamped slider block model, equation (8.1a) (Figure 8.5a, Table 2). That is, using the difference between the dashed lines in Figure 8.5a as a lengthening of event duration due to energy lost to radiation. On average the observed durations (Figure 8.5a, slider-block model fit line) are around 10% higher than expected (slider-block prediction line). The corresponding ratio of the predicted duration to the observed duration is $\Delta t_{obs}/\Delta t = 1.09$. To produce this relative increase requires a value of the impedance that is about 25% of product of the stiffness and the resonance time constant T as indicated by the dashed reference lines on Figure 8.A1. In terms of the observed event duration and average velocity, apparent stress for these experiments is

$$\tau_a = 0.22 \hat{V} k \Delta t_{obs}. \quad (8.A2c)$$

Resulting values from equation (8.A2c) using the tabled values of average velocity, stiffness, and duration (Table 8.2) range from 0.05 to 0.18 MPa. The estimated average radiation efficiency, the ratio of apparent stress to static stress drop [Savage and Wood, 1971], is 0.22. This ratio fixes the average slip overshoot, $\xi = 0.5 - \tau_a/\Delta\tau_s$ [Savage and Wood, 1971], to be 0.28. These results compare favorably with estimates for earthquakes, stick-slip experiments, and prior slider-block models [McGarr, 2012, and references therein].

REFERENCES

- Abe, K. (1975), Static and dynamic fault parameters of the Saitama earthquake of July 1, 1968, *Tectonophysics*, 27, 223–238.
 Baltay, A., S. Ide, G. A. Prieto, and G. C. Beroza (2011), Variability in earthquake stress drop and apparent stress, *Geophys. Res. Lett.*, 38, L06303, doi:10.1029/2011GL046698.

- Baltay, A., G. Prieto, and G. C. Beroza (2010), Radiated seismic energy from coda measurements indicates no scaling in apparent stress with seismic moment, *J. Geophys. Res.*, **115**, B08314, doi:10.1029/2009JB006736.
- Beeler, N. M. (2001), Stress drop with constant, scale independent seismic efficiency and overshoot, *Geophys. Res. Lett.*, **28**, 3353–3356.
- Beeler, N. M., B. Kilgore, A. McGarr, J. Fletcher, J. Evans, and S. R. Baker (2012), Observed source parameters for dynamic rupture with non-uniform initial stress and relatively high fracture energy, *Journal of Structural Geology* (Spec. Iss.), **38**, p. 77–89.
- Brace, W. F., and J. D. Byerlee (1966), Stick-slip as a mechanism for earthquakes, *Science*, **153**, 990–992.
- Brune, J. N. (1970), Tectonic stress and the spectra of seismic shear waves from earthquakes, *J. Geophys. Res.*, **75**, 4997–5009.
- Byerlee, J. D., and W. F. Brace (1968), Stick slip, stable sliding, and earthquakes: Effect of rock type, pressure, strain rate and stiffness, *J. Geophys. Res.*, **73**, 6031–6037.
- Di Toro, G., R. Han, T. Hirose, N. De Paola, K. Mizoguchi, F. Ferri, M. Cocco, and T. Shimamoto (2011), Fault lubrication during earthquakes, *Nature*, **471**, 494–499.
- Dieterich, J. H. (1978), Time-dependent friction and the mechanics of stick-slip, *Pure Appl. Geophys.*, **116**, 790–806.
- Johnson, T., F. T. Wu, and C. H. Scholz (1973), Source parameters for stick-slip and for earthquakes, *Science*, **179**, 278.
- Johnson, T. L., and C. H. Scholz (1976), Dynamic properties of stick-slip friction of rock, *J. Geophys. Res.*, **81**(5), 881–888, doi:10.1029/JB081i005p00881.
- Kanamori, H. (2001), Energy budget of earthquakes and seismic efficiency, in *Earthquake thermodynamics and phase transformations in the Earth's interior*, Edited by R. Teisseyre and E. Majewski, pp 293–305, Academic Press, New York.
- Kilgore, B. D., Blanpied, M. L., and Dieterich, J. H. (1993), Velocity dependent friction of granite over a wide range of conditions, *Geophys. Res. Lett.*, **20**, 903–906.
- Kilgore, B., J. Lozos, N. M. Beeler, and D. Oglesby (2012), Laboratory observations of fault strength in response to changes in normal stress, *Journal of Applied Mechanics* (Jim Rice Spec. Iss.), JAM-11-1213.
- Koizumi, Y., K. Otsuki, A. Takeuchi, and H. Nagahama (2004), Frictional melting can terminate seismic slips, experimental results of stick-slips, *Geophys. Res. Lett.*, **31**, L21605.
- Linker, M. F., and J. H. Dieterich (1992), Effects of variable normal stress on rock friction: Observations and constitutive equations, *J. Geophys. Res.*, **97**, 4923–4940.
- Lockner, D. A., B. D. Kilgore, N. M. Beeler, and D. E. Moore (2017), The transition from frictional sliding to shear melting in laboratory experiments, in *Fault zone dynamic processes: Evolution of fault properties during seismic rupture*, Edited by M. Y. Thomas, T. M. Mitchell, and H. S. Bhat, this volume, AGU, Hoboken, NJ.
- Lockner, D. A., D. E. Moore, N. M. Beeler, and B. D. Kilgore (2010), Surface Melt Produced on Faults During Laboratory Stick-Slip Experiments, Abstract T23A-2245, presented at 2010 Fall Meeting, AGU, San Francisco, Calif., 13–17 Dec.
- Lockner, D. A., and P. G. Okubo (1983), Measurements of frictional heating in granite, *J. Geophys. Res.*, **88**, 4313–4320.
- McGarr, A. (1994), Some comparisons between mining-induced and laboratory earthquakes, *Pure Appl. Geophys.*, **142**, 467–489.
- McGarr, A. (1999), On relating apparent stress to the stress causing earthquake fault slip, *J. Geophys. Res.*, **104**, 3003–3011.
- McGarr, A. (2012), Relating stick-slip friction experiments to earthquake source parameters, *Geophys. Res. Lett.*, **39**, L05303, doi:10.1029/2011GL050327.
- McGarr, A., and J. B. Fletcher (2001), A method for mapping apparent stress and energy radiation applied to the 1994 Northridge Earthquake Fault Zone—Revisited, *Geophysical Research Letters*, **28**, 3529–3532, doi:10.1029/2001GL013094.
- McLaskey, G. C., B. D. Kilgore, D. A. Lockner, and N. M. Beeler (2015), A robust calibration technique for acoustic emission systems based on momentum transfer from a ball drop, *Bulletin of the Seismological Society of America*, **105**, 257–271, doi:10.1785/0120140170.
- Rice, J. R. (1993), Spatio-temporal complexity of slip on a fault, *J. Geophys. Res.*, **98**, 9885–9907.
- Rice, J. R., and S. T. Tse (1986), Dynamic motion of a single degree of freedom system following a rate and state dependent friction law, *J. Geophys. Res.*, **91**, 521–530.
- Savage, J. C., and M. D. Wood (1971), The relation between apparent stress and stress drop, *Bull. Seismol. Soc. Am.*, **61**, 1381–1388.
- Shelly, D. R., G. C. Beroza, S. Ide, and S. Nakamura (2006), Low frequency earthquakes in Shikoku, Japan, and their relationship to episodic tremor and slip, *Nature*, **442**, 188–191, doi:10.1038/nature04931.
- Shimamoto, T., J. Handin, and J. M. Logan (1980), Specimen-apparatus interaction during stick-slip in a triaxial compression machine: A decoupled tow-degree of freedom model, *Tectonophysics*, **67**, 175–205.
- Singh, S. K., and M. Ordaz (1994), Seismic energy release in Mexican subduction zone earthquakes, *Bull. Seismol. Soc. Am.*, **84**, 1533–1550.
- Wald, D. J., T. H. Heaton, and K. W. Hudnut (1996), The slip history of the 1994 Northridge, California, earthquake determined from strong motion, teleseismic, GPS, and leveling data, *Bull. Seismol. Soc. Am.*, **86**, S49–S70.
- Walsh, J. B. (1971), Stiffness in faulting and in friction experiments, *J. Geophys. Res.*, **76**, 8597–8598, doi:10.1029/JB076i035p08597.